Catalysis Today 442 (2024) 114908

Contents lists available at ScienceDirect

Catalysis Today

journal homepage: www.elsevier.com/locate/cattod

Different role of ruthenium and platinum defective sites on the catalytic activity for the hydrogen evolution reaction

Didac A. Fenoll, Mariona Sodupe, Xavier Solans-Monfort *

Departament de Química, Universitat Autònoma de Barcelona, Carrer dels Til·lers S/N, Bellaterra 08193, Spain

ARTICLE INFO

Keywords:
Hydrogen evolution reaction
Ruthenium
Platinum
DFT
Catalysis

ABSTRACT

The reduction of protons to H_2 (the hydrogen evolution reaction, or HER) is one of the two half reaction of water electrolysis. It produces H_2 that can be used as an energy vector or sustainable feedstock for other compounds. Platinum electrodes are the "golden standard" catalysts. However, due to Pt cost, there is a need for cheaper alternatives. Indeed, highly active ruthenium nanoparticles are a promising alternative. In this contribution, we use DFT (PBE-D2) calculations to understand the differences in the catalytic activities of Ru and Pt materials by considering slab models containing crystalline close packed planes, terraces, steps, islands and adatoms. Results reveal that the strong adsorption of isolated H atoms on either material and on various sites prevents the hydrogen evolution reaction from taking place. Regardless of the model considered, the formation of a monolayer is also too favorable, thus suggesting that higher coverages are needed before HER onset. The adsorption energies of H atoms exceeding the monolayer on platinum's crystalline surfaces, defective steps and terraces are very close to the ideal value, consistent with platinum's high catalytic activity. These results outline that the presence of lowly coordinated metal centers has little effect on the reactivity of Pt. The adsorption energy of extra H on Ru surfaces depends on the adsorption site: On non-defective sites, the adsorption of the extra H is unfavorable, leading to inefficient catalysts. In contrast, the adsorption on defective sites is favorable and close to the ideal value, thus suggesting an enhancement of the catalytic activity when Ru coordination decreases. These results outline that the reactivity toward hydrogen of Ru materials is more sensitive to surface morphology than Pt-based ones. Indeed, the presence of low coordinated centers is larger on Ru nanoparticles, thus rationalizing their high HER catalytic activity.

1. Introduction

Water electrolysis powered with renewable energies (including sunlight conversion) has long been envisioned as an ideal source of green hydrogen (H_2) [1–3]. Among the major applications of this sustainably produced H_2 are its use as an energy vector able to store sunlight energy in chemical bonds [4,5] as well as a feedstock reagent in many crucial industrial processes [6,7]. This includes the synthesis of green ammonia, which is seen as a promising alternative to the current Haber-Bosch process [8–10]

Water electrolysis implies two half reactions (Scheme 1): i) at the anode, water is oxidized to O_2 through the oxygen evolution reaction (OER); and ii) at the cathode, protons are reduced to H_2 in acidic media through the hydrogen evolution reaction (HER) [11,12]. Current efforts in HER upscaling mainly target the costly noble metals employed as electrocatalysts [11,13]. The so-called "golden standard" catalyst is platinum,[14] whose low Earth-abundance makes it costly. Several non-mutually exclusive strategies have been outlined to reduce the catalyst cost [15,16], including: a) the use of Earth-abundant alternatives to platinum [15,17–25] and b) the design of new materials with lower noble metal content [16,19,26–32]. In the struggle for Pt-free catalysts [14], advances in nanofabrication allow for finely-tuned catalysts to be designed, aided by the extensive research into single-atom catalysts (SAC) [28,30,31,33–35] and SAC-alloys [36], edged surfaces [37] and nanoparticles [38]. In this context, despite also being a noble metal, ruthenium has attracted significant attention [12,39,40]. Indeed, ruthenium-based materials can be used as catalysts for the hydrogen evolution reaction in the form of small nanoparticles with high catalytic activities that in some cases are close to those of platinum-based materials [13,27,41–49]. The catalytic activity of ruthenium nanoparticles has been reported to depend on the nature of the capping ligands [46] and on surface amorphization [41] both being indicative of high

* Corresponding author.
E-mail address: xavier.solans@uab.cat (X. Solans-Monfort).

https://doi.org/10.1016/j.cattod.2024.114908
Received 21 February 2024; Received in revised form 30 May 2024; Accepted 19 June 2024
Available online 27 June 2024

Oxygen Evolution Reaction

$$2\,H_2O \longrightarrow O_2 + 4\,H^+ + 4\,e^-$$

Hydrogen Evolution Reaction

$$2\,H^+ + 2\,e^- \longrightarrow H_2$$

$$E^o = 0.0\ V \text{ and } E_{H+} = 1/2\,E_{H2}$$ **CompHSE**

Scheme 1. Water electrolysis half reactions.

sensitivity to surface morphology. Nevertheless, despite the sizeable number of contributions analyzing the catalytic activity for HER of ruthenium [27,39,41,43,44,47,50–54] there is not a systematic computational study describing how the catalytic activity is influenced by surface morphology.

Computational chemistry is essential to state-of-the-art material screening in electrocatalysis [11,55]. It has been applied to determine the catalytic activity – metal correlations [34,56,57] and to provide an atomistic understanding of the catalytic activity at different sites on a specific material [58,59]. Most of these contributions (particularly those involving acidic media) are based on the Nørskov model [11,60], which uses the hydrogen adsorption energy (computed through the computational hydrogen standard electrode (CompHSE) [61] Scheme 1) as the key descriptor for predicting the catalytic activity of a particular material and site [11,60]. In this approach, hydrogen adsorption should be neither too weak (H is not adsorbed at reaction conditions) nor too strong (H_2 formation and desorption are hindered by metal-H interactions). Assuming constant thermal contributions, the optimal value is proposed to be around -0.24 eV (-23 kJ mol^{-1}), which fits with the value computed for Pt, but differs significantly from that of ruthenium. Remarkably, although in their seminal work Nørskov and co-workers considered different H coverages on the metallic surfaces [60], most of subsequent work [62] considered the adsorption energies at low coverages, without exceeding unity. More recently, some contributions showed that, at least in the case of ruthenium, coverages exceeding one H per surface metal site are needed to reproduce the experimental trends, both when using slab [41,63,64] and nanoparticle models [27,65].

The influence of surface morphology and active site metal coordination on the HER catalytic activity has been widely analyzed for Pt based materials, either using slab models [58,66] and nanoparticles [38]. Results show that catalyst activity for HER is sensitive to the active site metal coordination environment, the highest activities being associated with metals coordinated to about 9 other centers [62,66]. To the best of our knowledge an analogous study on ruthenium-based or other metal materials has never been performed. Furthermore, a comparison between different materials as a function of the coordination environment has not been reported.

In this contribution, we analyze the catalytic activity of Ru and Pt sites of different slab models including pure crystalline environments, steps, terraces, islands and adatoms with the aim of determining the most active sites for ruthenium and how they compare to equivalent sites on platinum. Catalytic activity is analyzed using the hydrogen adsorption energy as descriptor at three different coverages: i) isolated H adsorption; ii) H monolayer formation and iii) H adsorption exceeding the monolayer. Results show that coverages exceeding the monolayer are required to obtain H adsorption energies close to those of the ideal value. Moreover, all Pt models lead to very similar adsorption energies, thereby suggesting that inclusion of defects has a minor role in enhancing the Pt catalytic activity. In contrast, adsorption energies on Ru-based materials are highly sensitive to metal coordination. Particularly, the presence of steps and islands is of high importance to enhance HER activity with Ru-based materials, something that can be achieved through nanoparticle design. Overall, the final estimated overpotential for Ru defective models are reasonably close to those of all Pt slabs.

2. Computational details

All simulations were performed with the VASP code, which employs three-dimensional periodic calculations using plane wave basis sets. For that, a vacuum space of at least 15 Å is set to avoid unrealistic interactions between images in the non-periodic direction of the slab models.

2.1. Models

The most stable *fcc* Pt(111) and *hpc* Ru(100) surfaces were used to model the non defective materials. The models of these pure crystalline surfaces (referred as $\mathbf{M_{20}}$ hereafter, M = Pt or Ru) were built as $5x2\sqrt{(2R\_(30°))}$ supercells. This supercell is rectangular and includes 20 surface atoms of a close packed plane. The slab thickness is fixed to 9 and 8 layers for Pt and Ru respectively (Fig. 1a). Additionally, three other surface models containing steps, terraces, islands and adatoms were also considered (Fig. 1b). They were built by carving out the desired pattern on both sides of the surface slab, which results in a reduction of thickness by two layers. The three new models are referred as: i) $\mathbf{M_{10}}$, which has 10 atoms on the uppermost layer with a terrace and a step between two planes; ii) $\mathbf{M_7}$, which has 7 atoms on the uppermost layer defining an island with a central nine coordinated metal; and iii) $\mathbf{M_1}$, which consists of a single adatom.

In line with previous contributions [41], an exhaustive exploration of hydrogen surface coverage (θ) has been undertaken, from single-hydrogen binding to coverages beyond monolayer formation. Upwards of 20 hydrogen atoms were needed to form a monolayer on the slab models. Adsorption energies were computed assuming the computational hydrogen standard electrode [61] and considering different coverages. For H adsorptions below θ = 1, hydrogen adsorption energies (E_{ads}) with respect to the pristine surface were calculated as follows:

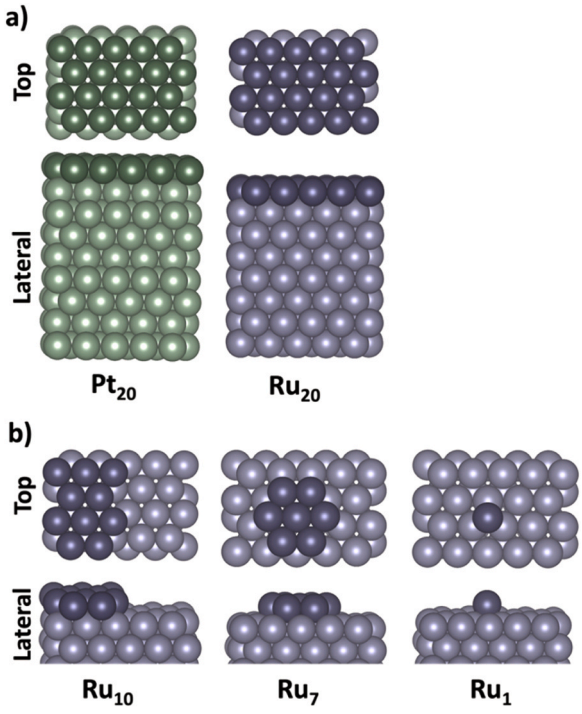

Fig. 1. Surface slab models used to represent crystalline and defective Pt and Ru materials. The dark color of the outermost metals is intended to better illustrate the represented defects.

$$E_{ads} = \frac{1}{n}\left(E_{nH-surf} - E_{surf} - \frac{n \cdot E_{H_2}}{2}\right)$$

Where E_{surf}, $E_{nH-surf}$ and E_{H_2} correspond to the PBE-D2 energies of the pristine surface, the surface with n adsorbed hydrogen atoms, and the dihydrogen molecule, respectively. In contrast, for a given coverage exceeding $\theta = 1$, the reference situation is the H monolayer and thus, the adopted expression is:

$$E_{ads} = E_{(N+1)H-surf} - E_{NH-surf} - \frac{E_{H_2}}{2}$$

Where $E_{(N+1)H-surf}$ corresponds to the energy of the uttermost hydrogen adsorption.

2.2. Level of theory

All calculations were performed at the density functional theory (DFT) level with the Perdew-Burke-Erzernhof (PBE) exchange-correlation functional [67], as implemented in VASP [68,69]. Dispersion interactions were introduced through Grimme's D2 correction [70].

The selection of D2 is grounded on prior experience with related materials and the observation that D2 tends to more accurately reproduce cell parameters for similar systems[71–73]. Magnetization was confirmed to be absent in the explored systems. Thus all simulations were conducted without introducing spin-polarization. Projector augmented wave (PAW) pseudopotentials [74,75] were used to represent the atomic cores, with plane waves utilizing a kinetic energy cut-off of 500 eV to describe the valence electrons. A fixed 2x2x1 Monkhorst-Pack [76] k-point grid was used in all calculations.

3. Results and discussion

The results and discussion section is organized as follows. We first focus on the H adsorption energies on pristine crystalline Pt and Ru slabs, paying special attention to different coverages (isolated H adsorption, H monolayer formation and adsorption of H exceeding the monolayer) and potential adsorption sites. Secondly, we describe the adsorption of H on the different sites present on the defective slab models **M$_1$**, **M$_7$** and **M$_{10}$** (M = Pt or Ru), encompassing the three aforementioned coverages. The nomenclature used herein to describe the adsorption sites is based on one or two letters followed by a set of numbers enclosed in parenthesis. Letters denote the specific adsorption site as follows: i) T, when it is on top of a surface atom; ii) Oh, on top of an octahedral hole; iii) Td, on top of a tetrahedral hole and iv) μ on a bridge between two surface atoms. Numbers indicate the coordination number of the metal atoms interacting with the adsorbed H. For Top sites, where only one atom interacts with H, a single number is provided. For bridge sites, two numbers are mandatory to describe the coordination number of the atoms interacting with H. Finally, for Oh and Td sites, three numbers are required, one for each metal interacting with H.

3.1. Pure crystalline M_{20} slabs

The adsorption of hydrogen on the pure crystalline models was briefly reported in a previous contribution of our group [41]. Here, we summarize the main results with the aim of using them as reference values for understanding the role of defects in the HER catalytic activity.

3.1.1. $\theta = 1/20$

Fig. 2 shows the optimized structures and the corresponding adsorption energies of one H atom on the two metallic surfaces. Fig. 3 reports the most stable structures and energetics of coverages $\theta = 1$ as well as the H adsorption energy of one H atom exceeding the most favorable monolayer on each metal.

The adsorption of one H atom on Pt is exoergic for all four potential sites (T(9), Oh(9,9,9), Td(9,9,9) and μ(9,9)). The associated adsorption energy range between −61.0 and −55.2 kJ mol^{-1}, with a marginal preference for octahedral sites (Oh(9,9,9)). These values are between 15 and 30 kJ mol^{-1} more negative than most of the previously reported energies for Pt that do not include dispersion corrections.[60,77] However, the differences between our data and the published values is much smaller when comparing with values including Grimme (D3) correction.[78] The adsorption of one H on Ru is only a minimum of the potential energy surface on the Oh(9,9,9) and Td(9,9,9) positions, thus indicating a clear preference for H adsorbing between three metals. The computed adsorption energies are −70.0 and −62.5 kJ mol^{-1}. Remarkably, the same preference for Oh(9,9,9) and Td(9,9,9) in ruthenium crystalline models was reported before.[63,64] Overall, the adsorption of H is stronger on Ru than on Pt, both values being significantly higher than the optimal value for HER (-23 kJ mol^{-1}). This suggests that HER does not take place at low coverages and thus, higher H concentrations need to be explored.

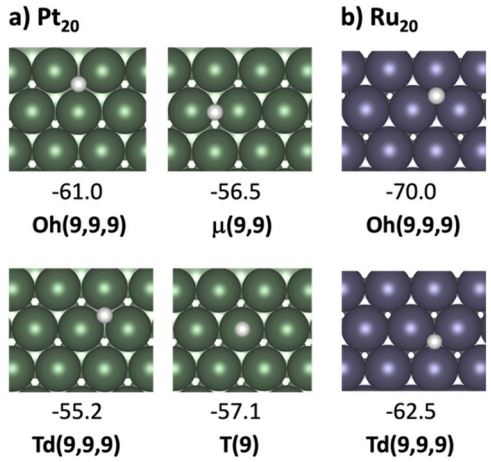

Fig. 2. Optimized structures and adsorption energies (in kJ mol^{-1}) of one hydrogen adsorption on a) **Pt$_{20}$** and b) **Ru$_{20}$** crystalline surfaces.

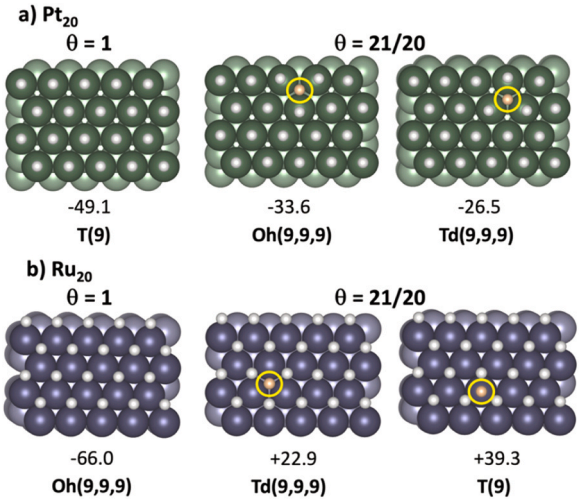

Fig. 3. Optimized structures and hydrogen adsorption energies (in kJ mol^{-1}) at coverages θ = 1 and θ =21/20 on a) **Pt$_{20}$** and b) **Ru$_{20}$**. The atom in orange corresponds to the H exceeding the monolayer.

3.1.2. $\theta = 1$

Adsorption of one H atom per surface metal on Pt leads to three potential monolayer structures (T, Oh and Td) (Fig. 3a reports the preferred one). The adsorption energies per H atom of the three

structures are again very similar (-49.1, −50.4 and −44.7 kJ mol^{-1} for T, Oh and Td, respectively) and show that θ = 1 on top and octahedral sites are essentially degenerate and both have a very minor preference over the Td monolayer. Again, the behavior for Ru is significantly different (Fig. 3b). In this case, only Oh and Td monolayers are minima of the potential energy surface, the former being more stable (-66.0 *vs.* −61.2 kJ mol^{-1}). Comparison between the adsorption energies of an isolated H atom with those of the monolayer shows a very minor impact from the presence of other adsorbed H atoms, at least up to this coverage. Indeed, the adsorption energies become less negative by only −11.9 and −4.0 kJ mol^{-1} for Pt and Ru respectively. Overall, H atoms forming a monolayer on Pt or Ru do not seem to be highly active due to their strong binding with the surface, thus suggesting that the adsorption of additional H atoms are required to perform the catalysis.

3.1.3. $\theta > 1$

Adsorption of one H atom exceeding the monolayer on Pt was studied starting from the monolayer with hydrogen atoms on top positions (Fig. 3a) as well as from the monolayer with hydrogen atoms on octahedral positions. We discuss in detail those results associated with the monolayer with all hydrogens on top as it is the preferred situation at coverages higher than 1. The adsorption energy of the H atom exceeding the monolayer is stable on the two explored sites (Oh(9,9,9) and Td (9,9,9)). The associated adsorption energies are −33.6 and −26.5 kJ mol^{-1}, respectively. These two values are very close to the reference value defined for an ideal catalyst, thus suggesting that HER activity starts when exceeding the monolayer. Conversely, for ruthenium close packed planes, the adsorption of the 21st atom is endoergic with values of +22.9 kJ mol^{-1} and +39.3 kJ mol^{-1} for the T(9) and Td (9,9,9) positions. Therefore, our results suggest that crystalline ruthenium would require high overpotentials to perform HER. Overall, results for the pure crystalline slab reproduce the observed trends, suggesting that Pt is a very active catalyst, while ruthenium is mostly inactive. In this context, exploration of how the presence of defects tunes the catalytic activity for HER of the two preceding materials may provide insights on the origin of the high catalytic activity of ruthenium nanomaterials.

3.2. *Defective M_{10}, M_7 and M_1 slabs*

The presence of terraces, steps, islands and adatoms implies that the 20 surface metal centers are no longer chemically equivalent. Consequently, the number of non-equivalent top, octahedral, tetrahedral and bridge sites increases. Fig. 4 shows the different metal sites present in the **M_{10}**, **M_7** and **M_1** models. For all these sites we computed the adsorption on top as well as on a representative set of octahedral, tetrahedral and bridge sites.

3.2.1. $\theta = 1/20$

Figs. 5 and 6 report the most stable structures of each type involving the adsorption of an isolated H atom on these models, both for Pt and for Ru. Tables 1 and 2 contain the adsorption energies of all considered sites on the Pt and Ru models.

The adsorption of one H atom on **Pt_{10}**, **Pt_7** and **Pt_1**, leads to adsorption energies ranging from −73.1 to −38.2 kJ mol^{-1}. The highest adsorption energies are generally obtained for bridge sites, while the

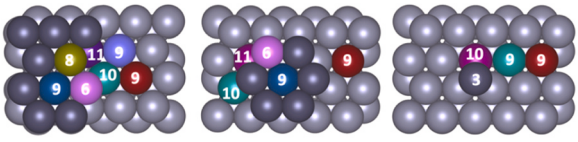

Fig. 4. Different surface metal centers on **M_{10}**, M_7 and **M_1** models. The number indicates the coordination number of each metal. The dark color of the outermost metals is intended to better illustrate the depth of the represented defects.

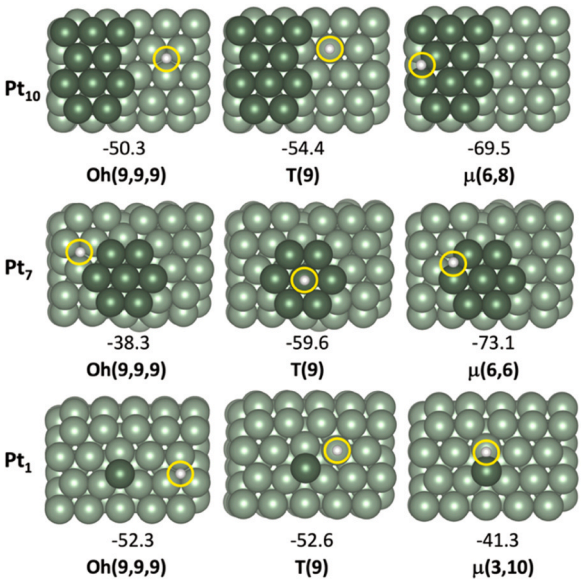

Fig. 5. Optimized structures and adsorption energies (in kJ mol^{-1}) for the most stable sites of each adsorption mode (octahedral hole (Oh), top (T) and bridge (μ)) on the three defective models of Pt (**Pt_{10}**, **Pt_7** and **Pt_1**). The dark color of the outermost metals is intended to better illustrate the depth of the represented defects.

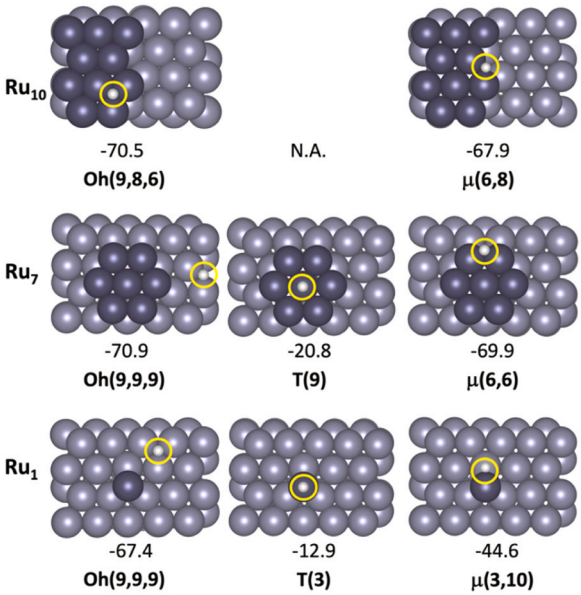

Fig. 6. Optimized structures and their adsorption energies (in kJ mol^{-1}) for the most stable sites of each adsorption mode (octahedral hole (Oh), top (T) and bridge (μ)) on the three defective models of ruthenium (**Ru_{10}**, **Ru_7** and **Ru_1**). The dark color of the outermost metals is intended to better illustrate the depth of the represented defects.

lowest values are found for T and some Td sites. This originates from a different behavior in the adsorption energies of each type of site as a function of the coordination of the metals involved. The adsorption energies (in absolute value) on T, Oh and Td sites tend to present a maximum when the coordination numbers of the metals involved is around that of the pure crystalline surface (9). For instance, while the adsorption on T9 ranges between −48.7 and −59.6 kJ mol^{-1}, the adsorption on top of the adatom (T3) is only −38.9 kJ mol^{-1}. Similarly, the adsorption on the non-defective Oh(9,9,9) is larger than −50.0 kJ mol^{-1}, but the adsorption on the less saturated Oh(9,6,6) is

Table 1
Adsorption energies (in kJ mol^{-1}) of one isolated H atom on the different sites of **Pt_{10}**, **Pt_7** and **Pt_1**. The most stable structure of each type of site is depicted in Fig. 5.

	Pt_{10}		Pt_7		Pt_1	
Type of site	Site	E_{ads}	Site	E_{ads}	Site	E_{ads}
Top	T(6)	-49.8	T(6)	-38.9 – −48.9	T(3)	-38.9
(-57.1)[a]	T(8)	-54.3	T(9)	-48.7 – −59.6	T(9)	-52.5 – −52.6
	T(9)	-51.1 – −54.4				
Oh	Oh(9,8,6)	-47.5	Oh(9,6,6)	-46.0	Oh(9,9,9)	-52.3
(-61.0)[a]	Oh(9,8,8)	-48.0	Oh(9,9,9)	-38.3	Oh(9,9,10)	-48.7
	Oh(9,9,9)	-50.3				
Td	Td(9,8,8)		Td(9,6,6)		Td(9,9,9)	-45.6
(-55.2)[a]	Td(9,9,9)	-44.2	Td(9,9,9)		Td(9,9,10)	-54.3
Bridge	μ(6,8)	-59.6 – −69.5	μ(6,6)	-73.1	μ(3,10)	-42.6
(-56.4)[a]	μ(6,10)	-66.4	μ(6,9)	-45.7		
			μ(6,10)	-59.1		
			μ(6,11)	-43.6		

[a] Computed adsorption energy for each type of site in the pure crystalline **Pt_{20}** model.

Table 2
Adsorption energies (in kJ mol^{-1}) of one isolated H atom on the different sites of **Ru_{10}**, **Ru_7** and **Ru_1**. The most stable structure of each type of site is depicted in Fig. 6.

	Ru_{10}		Ru_7		Ru_1	
Type of site	Site	E_{ads}	Site	E_{ads}	Site	E_{ads}
Top (N.A)[a]			T(9)	-20.8	T(3)	-12.9
Oh	Oh(9,8,6)	-70.5	Oh(9,6,6)	-60.8	Oh(9,9,9)	-67.4
(-70.0)[a]	Oh(9,8,8)	-53.0	Oh(11,6,6)	-50.9	Oh(10,9,9)	-57.0
	Oh(9,9,9)	-68.8	Oh(9,9,9)	-70.9		
Td	Td(9,8,6)		Td(9,6,6)		Td(9,9,9)	-59.8
(-62.5)[a]	Td(9,8,8)	-53.0	Td(9,9,9)		Td(10,9,9)	-47.2
	Td(9,9,9)	-62.0	Td(10,9,9)	-61.5		
			Td(11,9,9)	-51.3		
Bridge	μ(6,8)	-67.9	μ(6,6)	-69.9	μ(3,10)	-44.6
(N.A.)[a]	μ(6,10)	-67.7	μ(6,10)	-65.1		
	μ(6,11)	-60.5	μ(6,11)	-50.9		

[a] Computed adsorption energy for each type of site in the pure crystalline **Ru_{20}** model.

−46.0 kJ mol^{-1}. Meanwhile, the adsorption on bridge centers increases when reducing the coordination number of the metal centers interacting with H. Indeed, the strongest adsorption energies are obtained for μ(6,6) (-73.1 kJ mol^{-1}). Remarkably, since the adsorption energies on all sites are very similar in pure crystalline Pt, the fact that the adsorption is enhanced when reducing the coordination of the metals involved for bridge sites makes these positions become the preferred adsorption centers. Overall, most of the adsorbed H on these defective Pt surfaces present strong interactions with the surface and, few exceptions aside, calculations suggest that HER would only occur with a H monolayer on the surface.

The differences between Pt and Ru observed on crystalline surfaces influence the behavior on the defective surfaces. However, for each material, the trends in adsorption energies as a function of the coordination number of the metals involved in each type of site remain rather similar. The computed adsorption energies of an isolated H atom on various defective models of ruthenium range between −70.9 and −12.9 kJ mol^{-1}, which are very similar to those of defective Pt surface. This is due to the top and, particularly, bridge sites of Ru adsorbing H more weakly than the analogous sites of Pt. Consequently, while a few top sites become minima of the potential energy surface and their adsorption energies are slightly favorable, in most cases, the adsorption on top evolves to the adsorption on an octahedral, tetrahedral or bridge site. Moreover, some bridge sites also become stable in defective models, particularly when involving lowly coordinated sites. However, the computed adsorption energies (in absolute value) are still lower than those computed for most Oh(9,9,9) or related octahedral sites that overall are still the most stable ones. Since adsorption on Oh sites is not particularly favored when including defects, this means that Pt and Ru defective surfaces present similar adsorption energies to the crystalline ones. In any case, most sites still exhibit very strong adsorptions, thus suggesting that higher coverages are required for performing the HER.

3.2.2. $\theta \geq 1$

Results for higher coverage adsorptions are summarized in Table 3, which reports the adsorption energies of the monolayer and the adsorption of additional H atoms exceeding the monolayer. Moreover Figs. 7 (Pt) and 8 (Ru) show the structure of the monolayers as well as some representative structures of an additional H on adsorption sites differing from the environments already existing in **M_{20}**. In both figures, the adsorption energy per H atom in the case of the monolayer or the adsorption energy of the additional H atom are also reported. Remarkably, the monolayers of the **M_{10}**, **M_7** and **M_1** models are constructed adding one H atom at each preferred site of the crystalline structure (top for Pt, octahedral holes for Ru) and a few additional atoms on the defects that show high adsorption energies at low coverage (mainly bridge sites). For instance, one additional H is included on the adatom of **Pt_1** and **Ru_1**, leading to a monolayer formed by 21 H; while two, three or four additional H atoms are added in bridge sites for **Ru_{10}**, **Ru_7** and the two **Pt** models, respectively. To ensure that the adsorption of these 21–24 H atoms is favorable at reaction conditions and that they all adsorb similarly, we computed the mean adsorption energy of these H atoms and compared to the values for isolated H species. The mean adsorption energy for **Pt_{10}**, **Pt_7** and **Pt_1** is −52.4, −51.9 and −46.4 kJ mol^{-1}, respectively, while the mean adsorption energies for the analogous models for ruthenium are −58.6, −59.0 and −56.2 kJ mol^{-1} for **Ru_{10}**, **Ru_7** and **Ru_1**, respectively. Consequently, in all cases the adsorption energy per H atom is significantly larger than the reference value (-23 kJ mol^{-1}) and relatively close to the individual adsorption energies. This suggests that there is only a minor destabilizing effect when going from the isolated adsorption to the monolayer (as already seen for **M_{20}** models) and that the models constructed are representative of the composition of the surface at reaction conditions.

As for the crystalline models, we considered the adsorption of one additional hydrogen to the monolayer. We analyzed the adsorption of the extra H on sites that are equivalent to those found for the crystalline models (Oh(9,9,9) and Td(9,9,9)) as well as sites that are unique in the presence of defects. Regardless the metal considered, the adsorption environment of H in the Oh or Td sites close to a defect is essentially equivalent to that of the flat surfaces. Moreover, the top sites on the defective centers are partially bent towards the step between the outermost layer and the subsequent ones. Finally, two main classes of bridge sites can be identified, sites in which the additional H atom interacts with two defective metal centers of the outermost layers μ(8,6) or μ(6,6) and sites on which H is placed between two layers, thus

Table 3
Adsorption energies (in kJ mol^{-1}) of a H atom exceeding the monolayer on the different sites of $\mathbf{M_{10}}$, $\mathbf{M_7}$ and $\mathbf{M_1}$. Some selected structures are depicted in Figs. 7 and 8, for Pt and Ru, respectively.

Site	$\mathbf{Pt_{10}}$	$\mathbf{Pt_7}$	$\mathbf{Pt_1}$	$\mathbf{Ru_{10}}$	$\mathbf{Ru_7}$	$\mathbf{Ru_1}$
ML[a]	-52.4[d]	-51.9[d]	-46.4[d]	-58.6[d]	-59.0[c]	-56.2[d]
T(3)	N.A.	N.A.	-79.4/-57.1/+35.9[e]	N.A.	N.A.	-46.2/-26.4 [f]
T(6)	-25.1	-33.6	N.A.	-40.4	-14.4/-15.6	N.A.
Oh^b_{def}	-19.7/-18.2	-31.9/-32.4	N.A.	N.A.	N.A.	N.A.
Oh(9,9,9)	-31.2	-32.2	-44.1	N.A.	N.A.	N.A.
Oh^c_{exc}	—	-21.4	N.A.	N.A.	N.A.	N.A.
μ^b_{def}	-22.2	-46.2	N.A.	-43.6	N.A.	N.A.
μ^c_{exc}	——	N.A.	N.A.	-40.4	N.A.	N.A.

[a] ML stands for monolayer.
[b] Centers composed by metal centers that have coordination numbers lower than 9 Oh(9,8,6), Oh(9,8,8) and μ(6,8) for $\mathbf{M_{10}}$ or Oh(9,6,6) and μ(6,6) for $\mathbf{M_7}$.
[c] Centers composed by metal centers that have coordination number higher than 9 Oh(9,10,10) and μ(6,10) for $\mathbf{M_{10}}$ or Oh(9,9,10) and μ(6,10) for $\mathbf{M_7}$.
[d] Adsorption energy per H atom with respect to the clean surface.
[e] Adsorption of 1/2/3 H atoms exceeding the monolayer on the adatom.
[f] Adsorption of 1/2 H atoms exceeding the monolayer on the adatom.

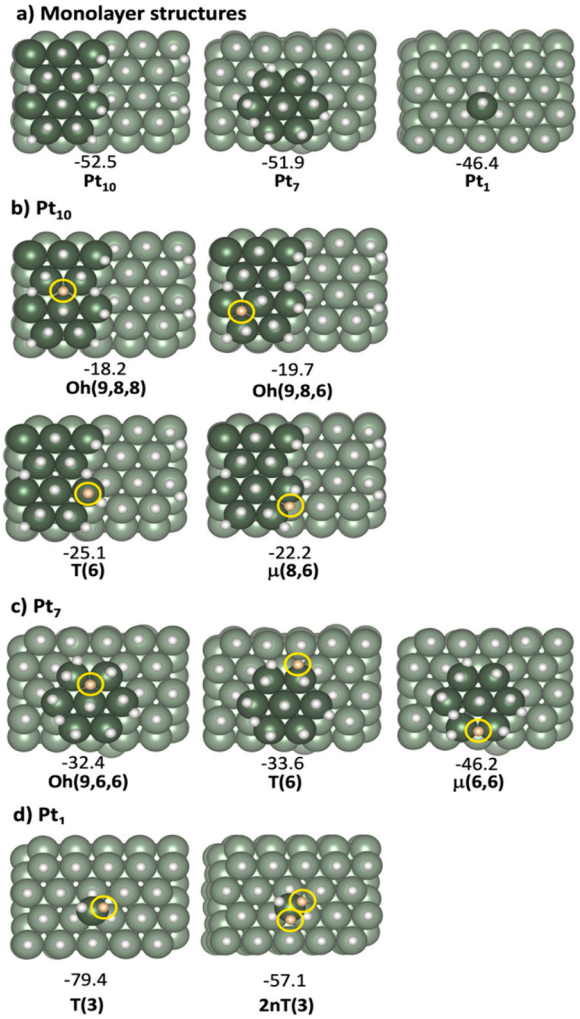

Fig. 7. Selected optimized structures and hydrogen adsorption energies (in kJ mol^{-1}) at a) coverages θ = 1 and exceeding the monolayer on b) $\mathbf{Pt_{10}}$, c) $\mathbf{Pt_7}$ and d) $\mathbf{Pt_1}$. The dark color of the outermost metals is intended to better illustrate the depth of the represented defects. The atom in orange corresponds to the H exceeding the monolayer.

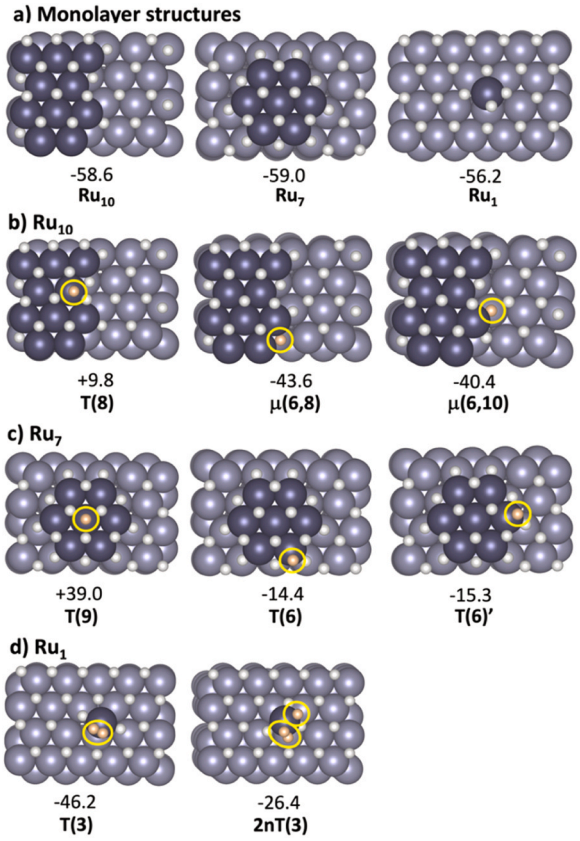

Fig. 8. Selected optimized structures and hydrogen adsorption energies (in kJ mol^{-1}) at a) coverages θ = 1 and exceeding the monolayer on b) $\mathbf{Ru_{10}}$, c) $\mathbf{Ru_7}$ and d) $\mathbf{Ru_1}$. The dark color of the outermost metals is intended to better illustrate the depth of the represented defects. The atom in orange corresponds to the H exceeding the monolayer.

interacting with a defective metal and another that is highly coordinated (μ(6,10)).

The adsorption of this extra H atom on different octahedral, bridge and top sites of $\mathbf{Pt_{10}}$ leads to adsorption energies between −31.2 and −18.2 kJ mol^{-1}. These values are very close to the ideal value and, in general, similar to the values obtained for crystalline surfaces. Remarkably, the defective sites present adsorption energies that are similar to the non-defective sites (compare T(6) and μ(6,8) adsorption energies (-25.1 and −22.2 kJ mol^{-1}) with that of Oh(9,9,9) (-31.2 kJ mol^{-1})). Overall, the adsorption energies closer to the ideal value correspond to T(6) and T(8) sites, but all sites diverge by less than 8 kJ mol^{-1} from the ideal value. As a consequence, calculations suggest that the inclusion of steps does not significantly improve the catalytic activity of Pt, although some defective sites seem to provide values

closer to the ideal value.

The adsorption of one H atom exceeding the monolayer on **Pt_7** was explored adsorbing the H on T(9), T(6) and Oh(9,6,6) as well as the basal Oh(9,9,9) and Oh(9,10,10) sites. The computed values range between −21.4 and −46.2 kJ mol^{-1}. As for the **Pt_{10}** model, all sites present very similar energies that span less than 10 kJ mol^{-1} around the ideal value. The only exception is μ(6,6), which was already predicted to be a strongly adsorbing site at low coverages. Therefore, the catalytic activity of the **Pt_7** model is also expected to be very high, but not particularly higher than that of **Pt_{20}** and **Pt_{10}**. Finally, the adsorption of one H atom exceeding the monolayer on **Pt_1** shows that the adatom is not an active center, even after adsorbing more than one extra H. Indeed, the adsorption energy of an additional H is −79.4 kJ mol^{-1}, that of the second H atom is −57.1 kJ mol^{-1}, while the adsorption of the third atom exceeding the monolayer is unfavorable. This is consistent with reports by Pacchioni and co-workers, which suggest that Pt single atom catalysts are not particularly active for HER [35,36].

Overall, defective Pt models present adsorption energies for H atoms exceeding the monolayer that are very close to the ideal value defined by Nørskov, thus suggesting that they are very active catalysts. However, comparison with the values obtained for crystalline Pt shows that the defective models are not particularly more active than the crystalline surface. That is, inclusion of defects does not substantially improve the catalytic activity of platinum.

The adsorption of an additional H atom on the monolayer of **Ru_{10}**, **Ru_7** and **Ru_1** presents a relatively different behavior to that found for platinum. The adsorption of the twenty-third H atom on **Ru_{10}** presents adsorption energies ranging from +29.3 to −43.6 kJ mol^{-1}. The adsorption of this additional H atom is unfavorable on those sites that resemble the crystalline Ru surface (T(9) and T(8)) but it is favorable in the more defective sites such as the T6 and the bridges (μ(8,6) and μ(10,6)). While the absolute value in these defective sites is still relatively large compared to the ideal value suggested by Nørskov, it is closer to the values obtained for crystalline ruthenium, thus suggesting that defective sites significantly enhance the catalytic activity of ruthenium for HER. Assuming that the kinetic effects are constant in both models and thus could be neglected, the computed overpotential would decrease around 0.2 V when including defects. A similar behavior is obtained for **Ru_7**. The adsorption energy of an additional H atom exceeding the monolayer on **Ru_7** ranges between +39.0 and −15.3 kJ mol^{-1}. Again, the crystalline T(9) sites present an unfavorable or negligible H adsorption while the more defective centers show the largest (in absolute value) adsorption energies. Particularly, the T(6) sites defining the step show adsorption energies that are only 10 kJ mol^{-1} lower than the ideal value. Finally, the adsorption of one additional atom on the adatom of **Ru_1** is favorable but the computed adsorption energy of −46.2 kJ mol^{-1} is relatively higher than the ideal value. Conversely, the adsorption of a second H atom leads to an adsorption energy of −26.4 kJ mol^{-1}, which seems to suggest that this center could be promising. That is, when three H atoms are adsorbed on the adatom, this center may start becoming active for HER. At this point it is worth mentioning that the addition of the extra H atom on T(3) leads to the formation of a dihydrogen intermediate, similar to the structure reported by Pacchioni and co-workers for some single atom catalysts [34].

Overall, calculations on **Ru_{10}**, **Ru_7** and **Ru_1** at a H coverage exceeding the monolayer show that the presence of defects significantly improves the catalytic activity of ruthenium-based materials for HER. Comparison with platinum shows that the catalytic activity of ruthenium is substantially more sensitive to surface morphology (with an overpotential decrease of at least 0.2 V) than Pt-based materials, where the presence of defects leads to very similar H adsorption energies compared to the crystalline slab. Said catalytic enhancement is associated with the presence of lowly coordinated metal centers (mainly six-coordinated sites) that can adsorb more than one hydrogen atom. Consequently, the high catalytic activity of ruthenium small nanoparticles could be attributed to the presence of a high number of lowly coordinated ruthenium centers, whose catalytic activity is only slightly below to that of platinum.

4. Conclusions

Platinum- and ruthenium-based materials are some of the most active catalyst for the hydrogen evolution reaction. In this contribution, we have analyzed how surface morphology influences their catalytic activity for HER by performing DFT (PBE-D2) calculations. For that, we have considered different slab models including crystalline close packed surfaces as well as the presence of terraces, steps, islands and adatoms. We used the H adsorption energy descriptor defined by Nørskov to estimate the catalytic activity of the different models. Additionally, several H coverages were considered, from the isolated adsorption of H to coverages exceeding the monolayer.

Results show that the adsorption of an isolated H atom on any of the considered models of Pt and Ru lead to a very strong interaction with the surface that prevents HER. Similarly, the adsorption of one H atom per surface metal also leads to exceedingly high (in absolute value) adsorption energies, thus suggesting that coverages beyond the monolayer are needed for HER to take place. The computed adsorption energies of H atoms exceeding the monolayer for crystalline Pt and Ru surfaces indicate that: a) the interaction of H with Pt at this coverage is optimal for performing HER very efficiently and b) the interaction of H at such a high coverage is unfavorable for ruthenium, thus predicting the need for high overpotentials. The addition of defects on Pt surfaces slightly optimizes the Pt – H interaction, which may be indicative of a marginal improvement of the HER activity on steps and islands. Remarkably, the catalytic activity enhancement is much larger in the case of ruthenium. The presence of lowly coordinated ruthenium centers favors the adsorption of additional H atoms with adsorption energies relatively close to the ideal value. Assuming a constant kinetic effect, calculations predict a decrease on the required overpotential of around 0.2 V. That is, ruthenium catalytic activity for HER is much more sensitive to surface morphology than that of platinum. Since the abundance of lowly coordinated ruthenium centers is expected to be significantly larger in small Ru nanoparticles, the present results provide a plausible explanation of the origin of their enhanced activity.

Funding

This work was supported by the Spanish Ministerio de Ciencia e Innovación [grant numbers: PID2020-112715GB-I00, FPU18/03612].

CRediT authorship contribution statement

Xavier Solans-Monfort: Writing – original draft, Supervision, Investigation, Formal analysis, Conceptualization. **Mariona Sodupe:** Writing – original draft, Supervision, Investigation, Formal analysis, Conceptualization. **Didac A. Fenoll:** Writing – original draft, Investigation, Formal analysis, Conceptualization.

Declaration of Competing Interest

All authors do not have any competing interest to declare.

Data availability

No data was used for the research described in the article.

Acknowledgements

The authors gratefully acknowledge financial support from MICINN [PID2020-112715GB-I00]. DAF acknowledges MICINN for his FPU PhD fellowship [FPU18/03612]. XSM is grateful for the Professor Agregat

Serra Húnter position. Authors thank Luis Rodríguez – Santiago for fruitful discussions.

References

[1] N.S. Lewis, Research opportunities to advance solar energy utilization, Science 351 (2016) aad1920, https://doi.org/10.1126/science.aad1920.

[2] J.A. Turner, Sustainable hydrogen production, Science 305 (2004) 972–974, https://doi.org/10.1126/science.1103197.

[3] J.O.M. Bockris, Hydrogen no longer a high cost solution to global warming: new ideas, Int. J. Hydrog. Energy 33 (2008) 2129–2131, https://doi.org/10.1016/j.ijhydene.2008.02.030.

[4] Z. Abdin, A. Zafaranloo, A. Rafiee, W. Mérida, W. Lipiński, K.R. Khalilpour, Hydrogen as an energy vector, Renew. Sustain. Energy Rev. 120 (2020) 109620, https://doi.org/10.1016/j.rser.2019.109620.

[5] N.S. Lewis, D.G. Nocera, Powering the planet: chemical challenges in solar energy utilization, Proc. Natl. Acad. Sci. 103 (2006) 15729–15735, https://doi.org/10.1073/pnas.0603395103.

[6] W. Lubitz, W. Tumas, Hydrogen: an overview, Chem. Rev. 107 (2007) 3900–3903, https://doi.org/10.1021/cr050200z.

[7] K.E. Lamb, M.D. Dolan, D.F. Kennedy, Ammonia for hydrogen storage; a review of catalytic ammonia decomposition and hydrogen separation and purification, Int. J. Hydrog. Energy 44 (2019) 3580–3593, https://doi.org/10.1016/j.ijhydene.2018.12.024.

[8] G. Hochman, A.S. Goldman, F.A. Felder, J.M. Mayer, A.J.M. Miller, P.L. Holland, L. A. Goldman, P. Manocha, Z. Song, S. Aleti, Potential economic feasibility of direct electrochemical nitrogen reduction as a route to ammonia, ACS Sustain. Chem. Eng. 8 (2020) 8938–8948, https://doi.org/10.1021/acssuschemeng.0c01206.

[9] D.R. MacFarlane, P.V. Cherepanov, J. Choi, B.H.R. Suryanto, R.Y. Hodgetts, J. M. Bakker, F.M.F. Vallana, A.N. Simonov, A roadmap to the ammonia economy, Joule 4 (2020) 1186–1205, https://doi.org/10.1016/j.joule.2020.04.004.

[10] M. Wang, M.A. Khan, I. Mohsin, J. Wicks, A.H. Ip, K.Z. Sumon, C.-T. Dinh, E. H. Sargent, I.D. Gates, M.G. Kibria, Can sustainable ammonia synthesis pathways compete with fossil-fuel based Haber–Bosch processes? Energy Environ. Sci. 14 (2021) 2535–2548, https://doi.org/10.1039/D0EE03808C.

[11] Z.W. She, J. Kibsgaard, C.F. Dickens, I. Chorkendorff, J.K. Nørskov, T.F. Jaramillo, Combining theory and experiment in electrocatalysis: insights into materials design, Science 1979 (355) (2017) eaad4998, https://doi.org/10.1126/science.aad4998.

[12] J. Yu, Q. He, G. Yang, W. Zhou, Z. Shao, M. Ni, Recent advances and prospective in ruthenium-based materials for electrochemical water splitting, ACS Catal. 9 (2019) 9973–10011, https://doi.org/10.1021/acscatal.9b02457.

[13] S. Zhang, J. Li, E.R. Wang, Recent progress of Ruthenium-based nanomaterials for electrochemical hydrogen evolution, ChemElectroChem 7 (2020) 4526–4534, https://doi.org/10.1002/celc.202001149.

[14] J.N. Hansen, H. Prats, K.K. Toudahl, N. Mørch Secher, K. Chan, J. Kibsgaard, I. Chorkendorff, Is there anything better than Pt for HER? ACS Energy Lett. 6 (2021) 1175–1180, https://doi.org/10.1021/acsenergylett.1c00246.

[15] X. Wang, Y.V. Kolen'ko, X. Bao, K. Kovnir, L. Liu, One-step synthesis of self-supported nickel phosphide nanosheet array cathodes for efficient electrocatalytic hydrogen generation, Angew. Chem. Int. Ed. 54 (2015) 8188–8192, https://doi.org/10.1002/anie.201502577.

[16] J. Song, Y. Kim, J. Lee, H.-J. Kim, Y.-E. Sung, T. Lim, O.J. Kwon, Implementation of proton exchange membrane water electrolyzer with ultralow Pt loading cathode through pt particle size control, ACS Sustain. Chem. Eng. 11 (2023) 16258–16266, https://doi.org/10.1021/acssuschemeng.3c04679.

[17] B. Hinnemann, P.G. Moses, J. Bonde, K.P. Jørgensen, J.H. Nielsen, S. Horch, I. Chorkendorff, J.K. Nørskov, Biomimetic hydrogen evolution: MoS2 nanoparticles as catalyst for hydrogen evolution, J. Am. Chem. Soc. 127 (2005) 5308–5309, https://doi.org/10.1021/ja0504690.

[18] X.L. Ho, H. Shao, Y.Y. Ng, R. Ganguly, Y. Lu, H.Sen Soo, Visible light driven hydrogen evolution by molecular nickel catalysts with time-resolved spectroscopic and DFT insights, Inorg. Chem. 58 (2019) 1469–1480, https://doi.org/10.1021/acs.inorgchem.8b03003.

[19] P. Wang, X. Zhang, J. Zhang, S. Wan, S. Guo, G. Lu, J. Yao, X. Huang, Precise tuning in platinum-nickel/nickel sulfide interface nanowires for synergistic hydrogen evolution catalysis, Nat. Commun. 8 (2017) 14580, https://doi.org/10.1038/ncomms14580.

[20] T.F. Jaramillo, K.P. Jørgensen, J. Bonde, J.H. Nielsen, S. Horch, I. Chorkendorff, Identification of active edge sites for electrochemical H2 evolution from MoS2 nanocatalysts, Science 317 (2007) 100–102, https://doi.org/10.1126/science.1141483.

[21] E.J. Popczun, J.R. McKone, C.G. Read, A.J. Biacchi, A.M. Wiltrout, N.S. Lewis, R. E. Schaak, Nanostructured nickel phosphide as an electrocatalyst for the hydrogen evolution reaction, J. Am. Chem. Soc. 135 (2013) 9267–9270, https://doi.org/10.1021/ja403440e.

[22] F. Ganci, V. Cusumano, P. Livreri, G. Aiello, C. Sunseri, R. Inguanta, Nanostructured Ni–Co alloy electrodes for both hydrogen and oxygen evolution reaction in alkaline electrolyzer, Int. J. Hydrog. Energy 46 (2021) 10082–10092, https://doi.org/10.1016/j.ijhydene.2020.09.048.

[23] J.F. Callejas, C.G. Read, E.J. Popczun, J.M. McEnaney, R.E. Schaak, Nanostructured Co2P electrocatalyst for the hydrogen evolution reaction and direct comparison with morphologically equivalent CoP, Chem. Mater. 27 (2015) 3769–3774, https://doi.org/10.1021/acs.chemmater.5b01284.

[24] S. Kong, P. Singh, G. Akopov, D. Jing, R. Davis, J. Perez-Aguilar, J. Hong, S.J. Lee, G. Viswanathan, E. Soto, M. Azhan, T. Fernandes, S. Harycki, A. Gundlach-Graham, Y.V. Kolen'ko, D.D. Johnson, K. Kovnir, Probing of the noninnocent role of P in transition-metal phosphide hydrogen evolution reaction electrocatalysts via replacement with electropositive Si, Chem. Mater. 35 (2023) 5300–5310, https://doi.org/10.1021/acs.chemmater.3c00460.

[25] R. Fernández-Climent, J. Redondo, M. García-Tecedor, M.C. Spadaro, J. Li, D. Chartrand, F. Schiller, J. Pazos, M.F. Hurtado, V. de la Peña O'Shea, N. Kornienko, J. Arbiol, S. Barja, C.A. Mesa, S. Giménez, Highly durable nanoporous Cu2–xS films for efficient hydrogen evolution electrocatalysis under mild pH conditions, ACS Catal. 13 (2023) 10457–10467, https://doi.org/10.1021/acscatal.3c01673.

[26] D. Astruc, F. Lu, J.R. Aranzaes, Nanoparticles as recyclable catalysts: the frontier between homogeneous and heterogeneous catalysis, Angew. Chem. Int. Ed. 44 (2005) 7852–7872, https://doi.org/10.1002/anie.200500766.

[27] J. Creus, J. DeTovar, N. Romero, J. García-Antón, K. Philippot, R. Bofill, X. Sala, Ruthenium nanoparticles for catalytic water splitting, ChemSusChem 12 (2019) 2493–2514, https://doi.org/10.1002/cssc.201900393.

[28] K. Jiang, B. Liu, M. Luo, S. Ning, M. Peng, Y. Zhao, Y.-R. Lu, T.-S. Chan, F.M.F. de Groot, Y. Tan, Single platinum atoms embedded in nanoporous cobalt selenide as electrocatalyst for accelerating hydrogen evolution reaction, Nat. Commun. 10 (2019) 1743, https://doi.org/10.1038/s41467-019-09765-y.

[29] J. Park, S. Lee, H. Kim, A. Cho, S. Kim, Y. Ye, J.W. Han, H. Lee, J.H. Jang, J. Lee, Investigation of the support effect in atomically dispersed Pt on WO3− x for utilization of Pt in the hydrogen evolution reaction, Angew. Chem. Int. Ed. 58 (2019) 16038–16042, https://doi.org/10.1002/anie.201908122.

[30] X. Cheng, Y. Li, L. Zheng, Y. Yan, Y. Zhang, G. Chen, S. Sun, J. Zhang, Highly active, stable oxidized platinum clusters as electrocatalysts for the hydrogen evolution reaction, Energy Environ. Sci. 10 (2017) 2450–2458, https://doi.org/10.1039/C7EE02537H.

[31] J. Zhang, Y. Zhao, X. Guo, C. Chen, C.-L. Dong, R.-S. Liu, C.-P. Han, Y. Li, Y. Gogotsi, G. Wang, Single platinum atoms immobilized on an MXene as an efficient catalyst for the hydrogen evolution reaction, Nat. Catal. 1 (2018) 985–992, https://doi.org/10.1038/s41929-018-0195-1.

[32] Y. Qu, B. Chen, Z. Li, X. Duan, L. Wang, Y. Lin, T. Yuan, F. Zhou, Y. Hu, Z. Yang, Thermal emitting strategy to synthesize atomically dispersed Pt metal sites from bulk Pt metal, J. Am. Chem. Soc. 141 (2019) 4505–4509, https://doi.org/10.1021/jacs.8b09834.

[33] J. Ji, Y. Zhang, L. Tang, C. Liu, X. Gao, Mi Sun, J. Zheng, M. Ling, C. Liang, Z. Lin, Platinum single-atom and cluster anchored on functionalized MWCNTs with ultrahigh mass efficiency for electrocatalytic hydrogen evolution, Nano Energy 63 (2019) 103849, https://doi.org/10.1016/j.nanoen.2019.06.045.

[34] G. Di Liberto, L.A. Cipriano, G. Pacchioni, Role of dihydride and dihydrogen complexes in hydrogen evolution reaction on single-atom catalysts, J. Am. Chem. Soc. 143 (2021) 20431–20441, https://doi.org/10.1021/jacs.1c10470.

[35] I. Barlocco, L.A. Cipriano, G. Di Liberto, G. Pacchioni, Modeling hydrogen and oxygen evolution reactions on single atom catalysts with density functional theory: role of the functional, Adv. Theory Simul. 6 (2023) 2200513, https://doi.org/10.1002/adts.202200513.

[36] I. Barlocco, G. Di Liberto, G. Pacchioni, Hydrogen complexes on single atom alloys: classical chemisorption versus coordination chemistry, Catal. Sci. Technol. 13 (2023) 5301–5312, https://doi.org/10.1039/D3CY00609C.

[37] I.T. McCrum, C.J. Bondue, M.T.M. Koper, Hydrogen-induced step-edge roughening of platinum electrode surfaces, J. Phys. Chem. Lett. 10 (2019) 6842–6849, https://doi.org/10.1021/acs.jpclett.9b02544.

[38] N. Cheng, S. Stambula, D. Wang, M.N. Banis, J. Liu, A. Riese, B. Xiao, R. Li, T. K. Sham, L.M. Liu, G.A. Botton, X. Sun, Platinum single-atom and cluster catalysis of the hydrogen evolution reaction, Nat. Commun. 7 (2016), https://doi.org/10.1038/ncomms13638.

[39] S.Y. Bae, J. Mahmood, I.Y. Jeon, J.B. Baek, Recent advances in ruthenium-based electrocatalysts for the hydrogen evolution reaction, Nanoscale Horiz. 5 (2020) 43–56, https://doi.org/10.1039/c9nh00485h.

[40] J. Zhu, L. Hu, P. Zhao, L.Y.S. Lee, K.-Y. Wong, Recent advances in electrocatalytic hydrogen evolution using nanoparticles, Chem. Rev. 120 (2019) 851–918, https://doi.org/10.1021/acs.chemrev.9b00248.

[41] N. Romero, D.A. Fenoll, L. Gil, S. Campos, J. Creus, G. Martí, J. Heras-Domingo, V. Collière, C.A. Mesa, S. Giménez, L. Francàs, L. Rodríguez-Santiago, X. Solans-Monfort, M. Sodupe, R. Bofill, K. Philippot, J. García-Antón, X. Sala, Ru-based nanoparticles supported on carbon nanotubes for electrocatalytic hydrogen evolution: structural and electronic effects, Inorg. Chem. Front. 10 (2023) 5885–5896, https://doi.org/10.1039/D3QI00698K.

[42] Z. Liu, X. Yang, G. Hu, L. Feng, Ru nanoclusters coupled on Co/N-doped carbon nanotubes efficiently catalyzed the hydrogen evolution reaction, ACS Sustain. Chem. Eng. 8 (2020) 9136–9144, https://doi.org/10.1021/acssuschemeng.0c02636.

[43] M. Fan, X. Chen, M. Zhang, L. Cui, X. He, X. Zou, Highly dispersed Ru nanoclusters anchored on B, N co-doped carbon nanotubes for water splitting, Inorg. Chem. Front. 9 (2022) 968–976, https://doi.org/10.1039/D1QI01672E.

[44] M. Zhang, J. Chen, H. Li, P. Cai, Y. Li, Z. Wen, Ru-RuO2/CNT hybrids as high-activity pH-universal electrocatalysts for water splitting within 0.73 V in an asymmetric-electrolyte electrolyzer, Nano Energy 61 (2019) 576–583, https://doi.org/10.1016/j.nanoen.2019.04.050.

[45] W. Luo, Y. Wang, C. Cheng, Mater. Ru-based electrocatalysts for hydrogen evolution reaction : recent research advances and perspectives, Today Phys. 15 (2020) 100274, https://doi.org/10.1016/j.mtphys.2020.100274.

[46] J. Creus, S. Drouet, S. Surinach, P. Lecante, V. Collière, R. Poteau, K. Philippot, J. Garcia-Anton, X. Sala, Ligand-capped Ru nanoparticles as efficient electrocatalyst for the hydrogen evolution reaction, ACS Catal. 8 (2018) 11094–11102, https://doi.org/10.1021/acscatal.8b03053.
[47] A. Moya, J. Creus, N. Romero, J. Alemán, X. Solans-Monfort, K. Philippot, J. García-Antón, X. Sala, R. Mas-Ballesté, Organocatalytic vs. Ru-based electrochemical hydrogenation of nitrobenzene in competition with the hydrogen evolution reaction, Dalton Trans. 49 (2020) 6446–6456, https://doi.org/10.1039/D0DT01075H.
[48] Q. Wang, M. Ming, S. Niu, Y. Zhang, G. Fan, J. Hu, Scalable solid-state synthesis of highly dispersed uncapped metal (Rh, Ru, Ir) nanoparticles for efficient hydrogen evolution, Adv. Energy Mater. 8 (2018) 1801698, https://doi.org/10.1002/aenm.201801698.
[49] Q. Hu, K. Gao, X. Wang, H. Zheng, J. Cao, L. Mi, Q. Huo, H. Yang, J. Liu, C. He, Subnanometric Ru clusters with upshifted D band center improve performance for alkaline hydrogen evolution reaction, Nat. Commun. 13 (2022) 3958, https://doi.org/10.1038/s41467-022-31660-2.
[50] B. Lu, L. Guo, F. Wu, Y. Peng, J.E. Lu, T.J. Smart, N. Wang, Y.Z. Finfrock, D. Morris, P. Zhang, N. Li, P. Gao, Y. Ping, S. Chen, Ruthenium atomically dispersed in carbon outperforms platinum toward hydrogen evolution in alkaline media, Nat. Commun. 10 (2019) 631, https://doi.org/10.1038/s41467-019-08419-3.
[51] M. Chen, T.J. Smart, S. Wang, T. Kou, D. Lin, Y. Ping, Y. Li, The coupling of experiments with density functional theory in the studies of the electrochemical hydrogen evolution reaction, J. Mater. Chem. A Mater. 8 (2020) 8783–8812, https://doi.org/10.1039/D0TA02549F.
[52] M. Cheng, H. Geng, Y. Yang, Y. Zhang, C.C. Li, Optimization of the hydrogen-adsorption free energy of ru-based catalysts towards high-efficiency hydrogen evolution reaction at all pH, Chem. Eur. J. 25 (2019) 8579–8584, https://doi.org/10.1002/chem.201900790.
[53] Y. Yang, Y. Yu, J. Li, Q. Chen, Y. Du, P. Rao, R. Li, C. Jia, Z. Kang, P. Deng, Y. Shen, Engineering ruthenium-based electrocatalysts for effective hydrogen evolution reaction, Nano Micro Lett. 13 (2021) 160, https://doi.org/10.1007/s40820-021-00679-3.
[54] D.H. Kweon, M.S. Okyay, S.-J. Kim, J.-P. Jeon, H.-J. Noh, N. Park, J. Mahmood, J.-B. Baek, Ruthenium anchored on carbon nanotube electrocatalyst for hydrogen production with enhanced Faradaic efficiency, Nat. Commun. 11 (2020) 1278, https://doi.org/10.1038/s41467-020-15069-3.
[55] F. Calle-Vallejo, M.T.M. Koper, First-principles computational electrochemistry: achievements and challenges, Electrochim. Acta 84 (2012) 3–11, https://doi.org/10.1016/j.electacta.2012.04.062.
[56] H. Xu, D. Cheng, D. Cao, X.C. Zeng, A universal principle for a rational design of single-atom electrocatalysts, Nat. Catal. 1 (2018) 339–348, https://doi.org/10.1038/s41929-018-0063-z.
[57] Z. Chen, J. Zhao, C.R. Cabrera, Z. Chen, Computational screening of efficient single-atom catalysts based on graphitic carbon nitride (g-C3N4) for nitrogen electroreduction, Small Methods 3 (2019) 1800368, https://doi.org/10.1002/smtd.201800368.
[58] F. Calle-Vallejo, D. Loffreda, M.T.M. Koper, P. Sautet, Introducing structural sensitivity into adsorption–energy scaling relations by means of coordination numbers, Nat. Chem. 7 (2015) 403–410, https://doi.org/10.1038/nchem.2226.
[59] P. Lindgren, G. Kastlunger, A.A. Peterson, A challenge to the G~ 0 interpretation of hydrogen evolution, ACS Catal. 10 (2019) 121–128, https://doi.org/10.1021/acscatal.9b02799.
[60] J.K. Nørskov, T. Bligaard, A. Logadottir, J.R. Kitchin, J.G. Chen, S. Pandelov, U. Stimming, Trends in the exchange current for hydrogen evolution, J. Electrochem Soc. 152 (2005) J23, https://doi.org/10.1149/1.1856988.
[61] J. Rossmeisl, Z.-W. Qu, H. Zhu, G.-J. Kroes, J.K. Nørskov, Electrolysis of water on oxide surfaces, J. Electroanal. Chem. 607 (2007) 83–89, https://doi.org/10.1016/j.jelechem.2006.11.008.
[62] F. Calle-Vallejo, J.I. Martínez, J.M. García-Lastra, P. Sautet, D. Loffreda, Fast prediction of adsorption properties for platinum nanocatalysts with generalized coordination numbers, Angew. Chem. Int. Ed. 53 (2014) 8316–8319, https://doi.org/10.1002/anie.201402958.
[63] L.A. Truflandier, I. Del Rosal, B. Chaudret, R. Poteau, I.C. Gerber, Where does hydrogen adsorb on ru nanoparticles? A powerful joint 2H MAS NMR/DFT approach, ChemPhysChem 10 (2009) 2939–2942, https://doi.org/10.1002/cphc.200900597.
[64] I. del Rosal, L. Truflandier, R. Poteau, I.C. Gerber, A density functional theory study of spectroscopic and thermodynamic properties of surfacic hydrides on Ru (0001) model surface: the influence of the coordination modes and the coverage, J. Phys. Chem. C 115 (2011) 2169–2178, https://doi.org/10.1021/jp110090e.
[65] J. Creus, S. Drouet, S. Suriñach, P. Lecante, V. Collière, R. Poteau, K. Philippot, J. García-Antón, X. Sala, Ligand-capped Ru nanoparticles as efficient electrocatalyst for the hydrogen evolution reaction, ACS Catal. 8 (2018) 11094–11102, https://doi.org/10.1021/acscatal.8b03053.
[66] M.D. Pohl, S. Watzele, F. Calle-Vallejo, A.S. Bandarenka, Nature of highly active electrocatalytic sites for the hydrogen evolution reaction at Pt electrodes in acidic media, ACS Omega 2 (2017) 8141–8147, https://doi.org/10.1021/acsomega.7b01126.
[67] J.P. Perdew, K. Burke, M. Ernzerhof, Generalized gradient approximation made simple, Phys. Rev. Lett. 77 (1996) 3865, https://doi.org/10.1103/PhysRevLett.77.3865.
[68] G. Kresse, J. Furthmüller, Efficient iterative schemes for ab initio total-energy calculations using a plane-wave basis set, Phys. Rev. B 54 (1996) 11169–11186, https://doi.org/10.1103/PhysRevB.54.11169.
[69] G. Kresse, J. Hafner, Ab initio molecular dynamics for liquid metals, Phys. Rev. B 47 (1993) 558–561, https://doi.org/10.1103/PhysRevB.47.558.
[70] S. Grimme, Semiempirical GGA-type density functional constructed with a long-range dispersion correction, J. Comput. Chem. 27 (2006) 1787–1799, https://doi.org/10.1002/jcc.20495.
[71] D. González, J. Heras-Domingo, S. Pantaleone, A. Rimola, L. Rodríguez-Santiago, X. Solans-Monfort, M. Sodupe, Water adsorption on MO2 (M = Ti, Ru, and Ir) surfaces. Importance of octahedral distortion and cooperative effects, ACS Omega 4 (2019) 2989–2999, https://doi.org/10.1021/acsomega.8b03350.
[72] D. González, J. Heras-Domingo, M. Sodupe, L. Rodríguez-Santiago, X. Solans-Monfort, Importance of the oxyl character on the IrO2 surface dependent catalytic activity for the oxygen evolution reaction, J. Catal. 396 (2021) 192–201, https://doi.org/10.1016/j.jcat.2021.02.026.
[73] D. González, M. Sodupe, L. Rodríguez-Santiago, X. Solans-Monfort, Surface morphology controls water dissociation on hydrated IrO 2 nanoparticles, Nanoscale 13 (2021) 14480–14489, https://doi.org/10.1039/D1NR03592D.
[74] P.E. Blöchl, C.J. Först, J. Schimpl, Projector augmented wave method: ab initio molecular dynamics with full wave functions, Bull. Mater. Sci. 26 (2003) 33–41, https://doi-org.are.uab.cat/10.1007/BF02712785.
[75] G. Kresse, D. Joubert, From ultrasoft pseudopotentials to the projector augmented-wave method, Phys. Rev. B 59 (1999) 1758, https://doi.org/10.1103/PhysRevB.59.1758.
[76] H.J. Monkhorst, J.D. Pack, Special points for Brillouin-zone integrations, Phys. Rev. B 13 (1976) 5188, https://doi.org/10.1103/PhysRevB.13.5188.
[77] W. Sheng, M. Myint, J.G. Chen, Y. Yan, Correlating the hydrogen evolution reaction activity in alkaline electrolytes with the hydrogen binding energy on monometallic surfaces, Energy Environ. Sci. 6 (2013) 1509–1512, https://doi.org/10.1039/C3EE00045A.
[78] O. Ahlstedt, J. Akola, Hydrogen evolution descriptors of 55-atom PtNi nanoclusters and interaction with graphite, J. Phys. Condens. Matter 36 (2024) 325001, https://doi.org/10.1088/1361-648X/ad4432.